FULL PAPER

3D Network Magnetophotonic Crystals Fabricated on *Morpho* Butterfly Wing Templates

Wenhong Peng, Shenmin Zhu, Wanlin Wang, Wang Zhang, Jiajun Gu, Xiaobin Hu, Di Zhang,* and Zhixin Chen*

A simple synthesis method combining a sol-gel route followed by a reduction step is developed for the fabrication of magnetophotonic crystal (MPC) materials from *Morpho* butterfly wings. The sol-gel route leads to hematite with a photonic crystal structure (PC-α-Fe_2O_3) being faithfully replicated from a biotemplate, and the desired magnetophotonic crystal Fe_3O_4 (MPC-Fe_3O_4) is obtained by the reduction of the PC-α-Fe_2O_3 under a H_2/Ar atmosphere. The structural replication fidelity of the process is demonstrated on both the macro- and microscale, and even down to the nanoscale, as evidenced by scanning electron microscopy, X-ray diffraction, reflectance measurements, and transmission electron microscopy. It is found that the chemical transformation of PC-α-Fe_2O_3 to MPC-Fe_3O_4 changes only the dielectric constant and does not induce structural defects that could affect the photonic-crystal properties of the composite. The photonic band gap of MPC-Fe_3O_4 can be red-shifted with an increase of the external magnetic field strength, which is further supported by theoretical calculations. The reported biomimetic technique provides an effective approach to produce magnetophotonic crystals from nature with 3D networks, which may open up an avenue for the creation of new magneto-optical devices and theoretical research in this field.

1. Introduction

Photonic crystals, having an optical analog of the energy gaps of semiconductors, enable control and manipulation of the flow of light for applications in the photonic and optical industries.[1–3] Using unique functional materials for photonic structural construction,[4] photonic band gaps can be switched or tuned by different external factors, such as electric[5] and magnetic fields,[6] temperature[7] or mechanical forces.[8] Particularly, research on tunable magnetophotonic crystal (MPC) systems that can control light beams by means of an external magnetic field are of great interest[9] for potential use in magnetic field sensors, optical switches and magneto-optical (MO) isolators.[10] A high MO response and a low propagation loss at longer wavelengths, as well as in the visible region, are crucial in practical MO devices. Strong photon confinement, associated with magnetic defects in magnetophotonic crystals, can be exploited to enhance and optimize MO Faraday rotation and the optical non-linearity of existing materials.[11] Much research effort has been made to synthesize MPCs, such as the coating of a SiO_2 opal template with a magnetic material,[12] multilayer sputtering[13] and electrochemical deposition on colloidal templates.[14] Though significant progress has been achieved, most research has focused only on introducing magnetic defects into existing opal photonic crystals.

Actually, 3D photonic crystals of ferromagnetic particles, such as Fe_3O_4, cannot be synthesized easily, in principle, because of the strong attractive magnetic interaction between the Fe_3O_4 particles. Recently, an assembly of superparamagnetic iron oxide colloidal particles was realized by using a ferrofluid in aqueous solution or nonpolar solvents.[9,15,16] During the process, surface coating with a metal or a layer of polyelectrolytes was necessary for the successful assembly of MPCs, in order to introduce electrostatic repulsive forces to balance the magnetic attractive force. This is the reason why the amount of experimental work on MPCs to confirm theoretical predictions is rather limited. More complex geometries, such as 3D biophotonic nanostructures, are still a challenge to model.

In fact, nature provides us a variety of photonic crystal structures that cannot be synthesized easily using available nanotechnology: arm ossicles from the light-sensitive brittle star species,[17] 2D pseudophotonic crystals in the hair-like setae of the polychete worm,[17] the macroporous photonic-crystal structures of parrot feathers,[18] a diamond-based photonic lattice discovered in beetles,[19] and a partial photonic band gap in the sea mouse showing remarkable coloration effects.[20] Particularly, butterfly wings are very well known for their diversity of colors and patterns, some of which derive from periodic surface scales of the wings. After millions of years of selection for a

W. Peng, Prof. S. Zhu, W. Wang, Dr. W. Zhang, Prof. J. Gu, Prof. X. Hu, Prof. D. Zhang
State Key Lab of Metal Matrix Composite
Shanghai Jiao Tong University
Shanghai, 200240, China
E-mail: smzhu@sjtu.edu.cn; zhangdi@sjtu.edu.cn
Dr. Z. Chen
Engineering Materials Institute
Faculty of Engineering
University of Wollongong
Wollongong, NSW2522, Australia

DOI: 10.1002/adfm.201103032

consistent optical function, photonic crystals in butterfly-wing scales are an ideal source to inspire biomimetic technology. More recently, a natural, magnetophotonic, nanocrystallite Fe_3O_4 in the Tagish Lake meteorite was reported,[21] which was formed 4.6 billion years ago. Unfortunately, an exact imitation of such biological structures by an artificial synthesis route is difficult, because the formation mechanism is tremendously complex and their exact nanoscale organization is uncertain. Replication is proven to be an efficient nanofabrication technique to obtain functional oxides with natural photonic structures. Our previous studies have shown that a direct biotemplate method can be used to synthesize various functional ceramic replicas with natural periodic structures, such as TiO_2,[22] ZnO[23] and ZrO_2 butterfly wings.[24] However, such approaches are not suitable for the direct fabrication of magnetophotonic crystals from a biotemplate. Herein, we address the above challenge by using the route of a sol-gel biotemplate then reduction. Using this method, we successfully fabricated magnetophotonic crystal Fe_3O_4 (MPC-Fe_3O_4) from *Morpho* butterfly wings. The photonic crystal structures of the obtained MPC-Fe_3O_4 and the intermediate hematite photonic crystals (PC-α-Fe_2O_3) were characterized by a series of measurements. The obtained MPC-Fe_3O_4 has a 3D network magnetophotonic crystal structure. The effect of an external magnetic field on the photonic band gap of the MPC-Fe_3O_4 in the visible light range was also investigated. It is shown that the reported biomimetic technique provides an effective approach for the synthesis of magnetic materials with photonic crystal structures, which is promising and significant for the investigation of magneto-optic properties.

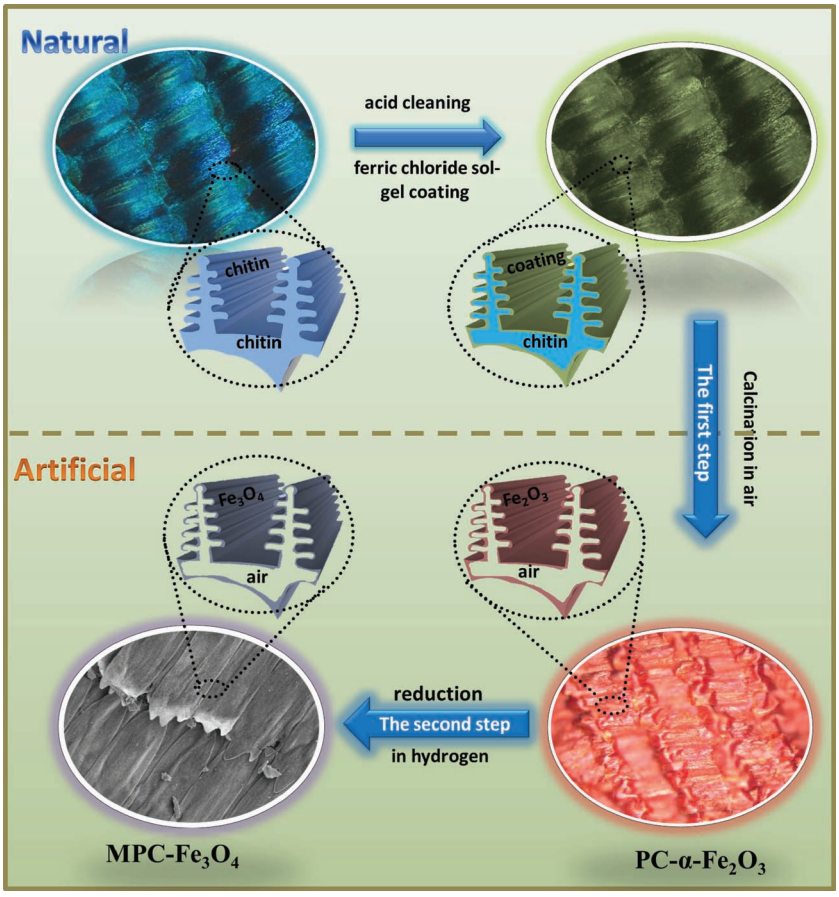

Scheme 1. Schematic illustration of the process of replicating 3D network magnetophotonic crystals from *Morpho* butterfly wings.

2. Results and Discussion

The overall process of MPC-Fe_3O_4 synthesis from *Morpho* butterfly wings is illustrated and described in **Scheme 1**: 1) the pretreated butterfly wings are immersed into a ferric chloride sol solution, allowing a sol-gel coating process; 2) the removal of the biotemplate at an elevated temperature produces hematite butterfly wings with a photonic crystal structure (PC-α-Fe_2O_3); and 3) the reduction of the PC-α-Fe_2O_3 in H_2/Ar results in magnetite butterfly wings with the same photonic crystal structure (MPC-Fe_3O_4).

The *Morpho* butterfly is a typical natural biological species, having a photonic crystal structure in its hierarchical nanoscales, which has been widely studied and systematically described.[25,26] The bright blue colors are produced by physical interactions of light with the photonic crystal structure in visible light (**Figure 1**a). The wings are composed of overlapping microscales, which form two or more layers over the wing membrane, like roof-tiles (Figure 1b). These overlapping scales have an overall rectangular shape. There are two different types of scale, as marked by the red square, type I, and the yellow square, type II, in Figure 1b. The fine distinctions between these two scales are revealed by the scanning electron microscopy (SEM) images shown in Figure 1c,d. Type I (or the basal scale[25]) gives a shining blue at most observation directions, while the appearance of type II (or the cover scale[25]) changes with the angle of observation from approximately transparent to light blue. The blue color of type I in Figure 1c results from arrays of vertically aligned, net-like skeleton structures. The dorsal surface of the scales consists of a network of parallel, longitudinal ridges joined together by slender, spaced cross-ribs that together form windows into the interior of the scales (Figure 1e). The wing scales of these butterflies consist of regular multilayer stacks that are made from alternating layers of cuticles and air, and they create intense structural colors. Figure 1d reveals that the typical dimensions of a type-II scale are a length of 150 μm and a width of 60 μm. Thirty-five to forty rows of lamellae are aligned on the scale surfaces, with an almost identical interspacing. Between the lamellae, supporting cross-ribs are present, each of which has one or two legs standing on the bottom surface and exhibits a hollow body. A closer view of these lamellae (ridges) is shown in Figure 1f. The ridges are decorated with nanoscale ribs that are spaced

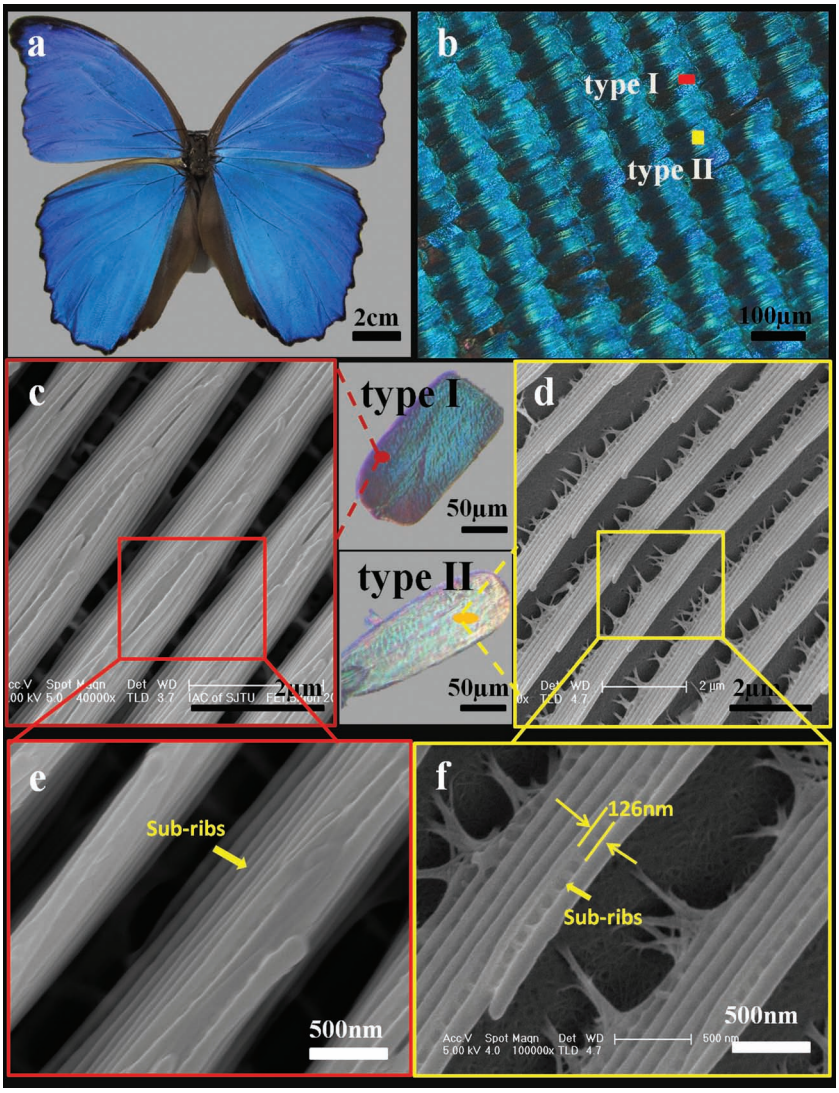

Figure 1. Characterization of natural *Morpho* butterfly wings from the macro- to nanoscale. a) Digital picture of intact butterfly. b) Optical microscopy image of the wing scales from the blue area, showing two different types of wing scale (type I, type II) on the surface. c and e) High-magnification SEM images of type-I scale. d and f) High-magnification SEM images of type-II scale.

approximately 126 nm apart. The structural colors are produced by genuine 3D biological photonic crystals comprising a complex network of the cuticular chitin dielectric (refractive index = 1.56) and the space covered by the scales of the wing. Thus, the two different overlapping scales give unique optical properties and fulfill distinct functions. The bright color and exquisite structure of *Morpho* butterfly wings are so interesting that we chose it as the hard template for our magnetophotonic crystals.

The morphologies of the MPC-Fe_3O_4 and the intermediate PC-α-Fe_2O_3 were firstly characterized using field-emission SEM (FE-SEM) (**Figure 2**). Both the PC-α-Fe_2O_3 (Figure 2a) and MPC-Fe_3O_4 (Figure 2f) replicas showed that the overall scale shape, the parallel ridges and the nanoscale ribs of the original *Morpho* butterfly wings were well maintained. The high-magnification images in Figure 2b,d reveal that the two different types of scale of the original biotemplate (type I and type II in Figure 1c,d) were also retained in the resultant PC-α-Fe_2O_3 replica. In particular, the excellent reproduction of the longitudinal ridges with overlapping, slanted lamellae running along the top of the ridges can clearly be seen in Figure 2c,e, corresponding to the original scales shown in Figure 1e,f, respectively. A small shrinkage of 21.8% was detected in the PC-α-Fe_2O_3 replica because of the elevated calcination temperature. Further reduction in H_2/Ar resulted in well-organized, periodic, hierarchical structures with nanoscale ribs, originating from the *Morpho* butterfly wings, in the obtained MPC-Fe_3O_4 (Figure 2f). Transverse ribs and microribs running down the sides of the longitudinal ribs can be clearly identified in the high-magnification SEM images in Figure 2g,i. Compared with the intermediate PC-α-Fe_2O_3 (Figure 2c,e), almost no shrinkage was detected in the MPC-Fe_3O_4 (Figure 2h,j). Thus, the complex, hierarchical structures of the original butterfly wings were preserved in the MPC-Fe_3O_4 during the two-step fabrication process.

Transmission electron microscopy (TEM) and high-resolution TEM (HR-TEM) images (**Figure 3**) provide further insight into the morphologies and microstructures of the PC-α-Fe_2O_3 (Figure 3a–d) and MPC-Fe_3O_4 (Figure 3e–h). The seamless, continuous shell at the contacting junction between the ridges and the scale bottom suggests that the PC-α-Fe_2O_3 (Figure 3a) and MPC-Fe_3O_4 (Figure 3e) retained the overall scale morphology of the original butterfly wing. The long rows in Figure 3b and 3f are the ridges orderly stacked by fastigiated parallel tubes. The thickness of the magnetite replica was approximately 100 nm (Figure 3f). The selected-area electron diffraction (SAED) pattern in Figure 3d indicates that the assembled units of the PC-α-Fe_2O_3 were polycrystalline in nature and the diffraction rings were indexed to the (102), (110), (113) and (300) planes; lattice fringes with interplanar distances d_{012} = 0.37 nm and d_{104} = 0.27 nm are obviously discernible in the HR-TEM images in Figure 3c. Electron diffraction and energy-dispersive X-ray (EDX) microanalysis of the PC-α-Fe_2O_3 (Figure S1, Supporting Information) suggests that the replica consisted of Fe and O elements and the carbon associated with the organic composition of the wing of the butterfly was almost completely removed by calcination. The HR-TEM analysis revealed that the thin-scale bottom comprised Fe_2O_3 nanocrystals approximately 23 nm in diameter (Figure S2, Supporting Information). The crystal structure of the MPC-Fe_3O_4 was determined from the SAED pattern (Figure 3h), which could be indexed consistently to the (111), (220), (311), (331) and (422) planes of spinal Fe_3O_4. The spacing between two adjacent lattice planes was about

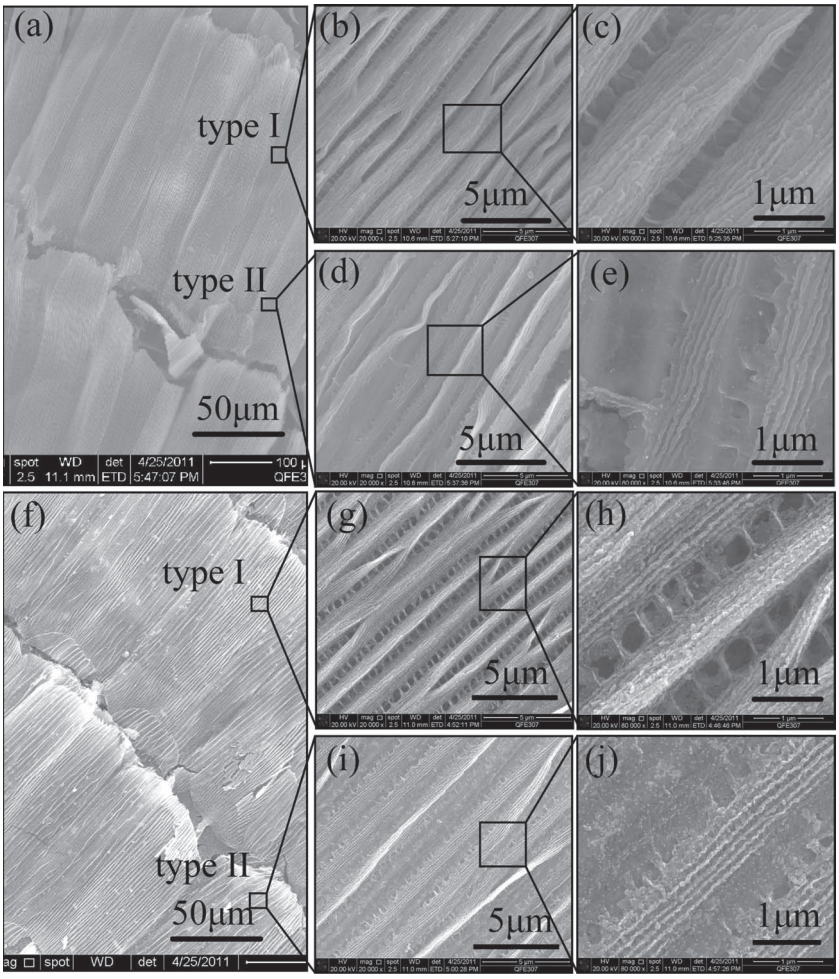

Figure 2. SEM images of the iron oxides. a) Low-magnification image of the PC-α-Fe_2O_3 replica. b,c) Different magnifications of a type-I scale of the PC-α-Fe_2O_3 replica. d,e) Different magnifications of a type-II scale of the PC-α-Fe_2O_3 replica. f) Low-magnification image of MPC-Fe_3O_4 reduced at 400 °C. g,h) Different magnifications of a type-I scale of the MPC-Fe_3O_4 replica. i,j) Different magnifications of a type-II scale of the MPC-Fe_3O_4 replica.

0.49 nm (Figure 3g), corresponding to the d_{111} of spinal Fe_3O_4. The fidelity of the fabrication process for the PC-α-Fe_2O_3 and MPC-Fe_3O_4 on the macro- and microscales and to the nanometer level was confirmed by TEM.

Figure 4 shows Raman spectra obtained from the intermediate PC-α-Fe_2O_3 and the final MPC-Fe_3O_4. The spectrum of the intermediate PC-α-Fe_2O_3 (spectrum a in Figure 4) exhibits bands characteristic of the hematite structure at 222, 241, 290, 406, 495 and 610 cm^{-1}. The Raman spectrum of the MPC-Fe_3O_4 (spectrum b in Figure 4) exhibits a main band centered at 664 cm^{-1}, which is in good agreement with the position reported in the literature for magnetite.[27] The band position at 532 cm^{-1} (spectrum b in Figure 4) and the presence of no other bands further confirmed the pure magnetite of the final product.

X-ray photoelectron spectroscopy (XPS) was conducted to confirm further the formation of Fe_3O_4 in the MPC-Fe_3O_4 (Figure S3, Supporting Information). **Figure 5** shows the Fe2p spectra of the PC-α-Fe_2O_3 and MPC-Fe_3O_4 replicas. As for the intermediate PC-α-Fe_2O_3, distinct peaks at 710.7 and 724 eV (spectrum a in Figure 5) and a satellite peak at around 718 eV were observed, which indicates that the iron was almost completely in the Fe^{3+} state in the PC-α-Fe_2O_3 replica.[28] The presence of Fe^{2+} in the MPC-Fe_3O_4 is indicated by the disappearance of the satellite peak at around 718 eV, between the two main Fe2p peaks (arrow in Figure 5). The Fe2p3/2 peak of the MPC-Fe_3O_4 replica at around 710 eV could be deconvoluted into three peaks at 708.2, 710.7 and 713.3 eV, using a least-squares curve-fitting method with a mixture of Gaussian and Lorentzian functions on a Shirley type background, as shown in Figure 5 (inset). The lower binding-energy at 708.2 eV was attributed to Fe^{2+} ions, while the binding energies at 710.7 and 713.3 eV were ascribed to Fe^{3+} ions in the MPC-Fe_3O_4, which is consistent with the reported results.[28] Therefore, the obtained MPC-Fe_3O_4 consisted of almost pure magnetite.

From the analysis of the FE-SEM, the TEM and the Raman spectra, it is reasonable to conclude that biomimetic magnetophotonic crystals were realized in the Fe_3O_4 butterfly wings by using this sol-gel then reduction process. The benefit of this sol-gel process to the morphology of the MPC-Fe_3O_4 was investigated further. A simple impregnation with aqueous $Fe(NO_3)_3$ solution, instead of using the ferric chloride alcohol sol, was used to fabricate Fe_2O_3 then MPC-Fe_3O_4. The same intermediate Fe_2O_3 (PC-α-Fe_2O_3) and final Fe_3O_4 (MPC-Fe_3O_4) were also observed in samples prepared by this simple impregnation and reduction process (Figure S4, Supporting Information). Therefore there was little difference between the samples prepared using these two methods, in terms of phase. However the Fe_2O_3 butterfly wing scales were bent and the aggregated particles were distributed non-uniformly on the ridges (Figure S5, Supporting Information) in the PC-α-Fe_2O_3 sample produced using the aqueous-$Fe(NO_3)_3$-solution impregnation. In the subsequent reduction process, the structure of the final MPC-Fe_3O_4 collapsed, as evidenced by the TEM images (Figure S6, Supporting Information). This was probably due to the fact that the ferric nitrate aqueous solution could not combine effectively with the active sites of the original butterfly wings. Thus, a sol solution is much better than an aqueous solution, in terms of structural integrity and morphology of the final Fe_3O_4 butterfly wings. In our experiment, we chose ferric chloride alcohol solution to form the sol solution. During the sol-gel process, the color of the iron chloride alcohol solution slowly changed from light yellow to transparent deep brown when it was heated at 60 °C for 15 min, indicating the formation of the sol-gel. It should be noted that a long-time treatment of the sol solution should be

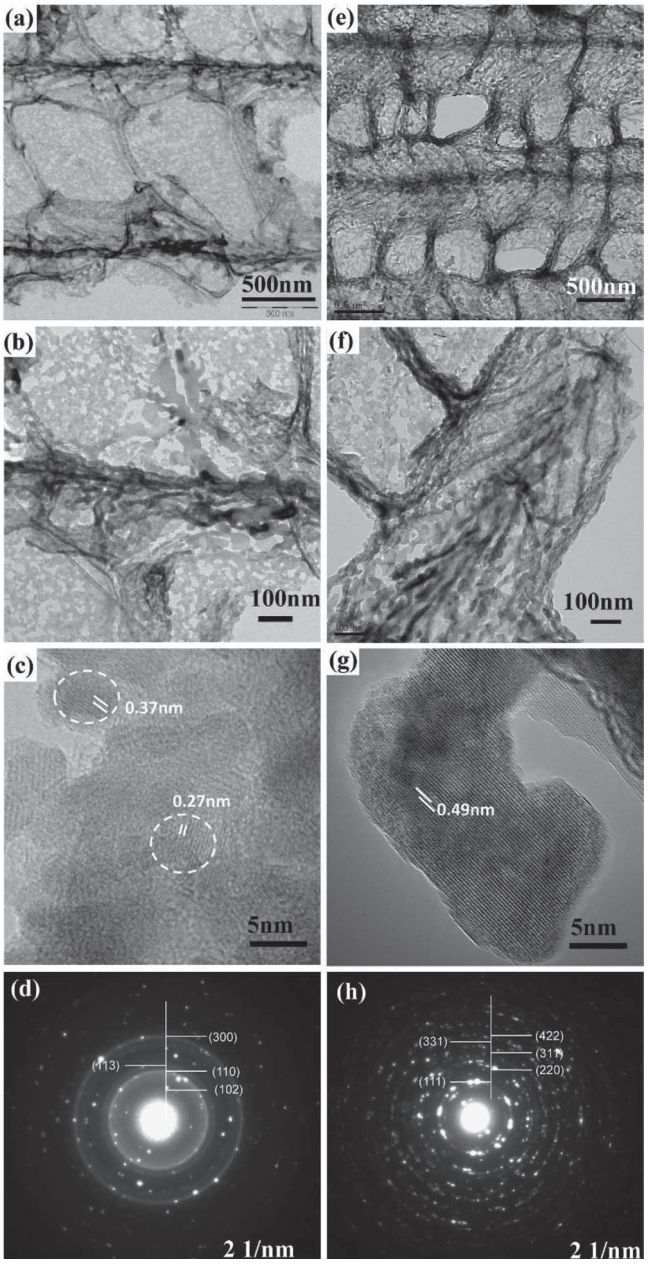

Figure 3. a–c) TEM images of PC-α-Fe_2O_3 replica. d) Corresponding SAED pattern of the PC-α-Fe_2O_3 replica. e–f) TEM images of the MPC-Fe_3O_4 replica. h) Corresponding SAED pattern of the MPC-Fe_2O_3 replica.

avoided because the transparent deep-brown solution will turn to reddish brown with a suspension of nanoparticles, which is not suitable for subtle replication.

The interaction between chitin and the sol solution could be analyzed using Fourier transform IR (FTIR) spectroscopy. The original butterfly wings are made up of protein and chitin, as evidenced by the FTIR-spectroscopy results (**Figure 6**). The absorption bands at 1655 and 1543 cm^{-1} were assigned to the amide I (primarily C–O stretch) and amide II (primarily NH in-plane bend plus CN stretch) of the protein, respectively.[29] The bands at 1157, 1115, 1074 and 1030 cm^{-1} might be the

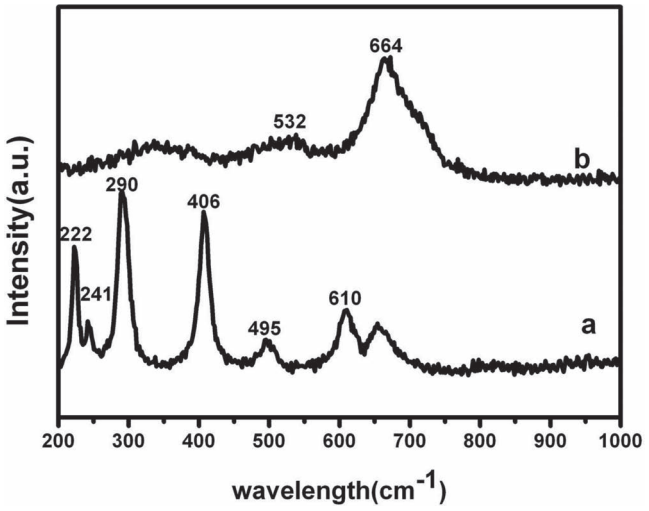

Figure 4. Raman spectra of the intermediate PC-α-Fe_2O_3 (a) and the final product MPC-Fe_3O_4 (b).

vibrational motion of the characteristic C–O bonds of the chitin.[29] After washing with acid, the negative amide in the wings was a little stronger, compared with the original wings, which provided more reactive functional groups for complexing with the positively charged Fe^{3+} in the sol, through electrostatic interactions. After dipping into the precursor, the intensity of the band at 3282 cm^{-1} decreased (O–H stretch vibration), along with a small shift to 3274 cm^{-1} (Figure S7, Supporting Information), which may be due to band formation between the sol-gel and the active surface of the original butterfly wing.

The intensity of the –COO– band at 1546 cm^{-1} weakened and the C–O-stretch vibration at 1031 cm^{-1} shifted to 1024 cm^{-1}, indicating a complex reaction between the sol solution and the

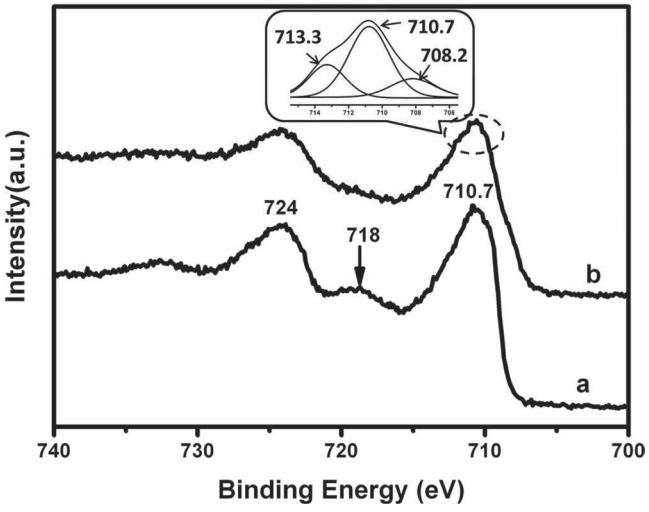

Figure 5. XPS spectra of the PC-α-Fe_2O_3 replica (a) and the MPC-Fe_3O_4 replica (b). The arrow indicates a satellite peak, which is characteristic of Fe^{3+}. The inset shows the deconvolution of the Fe2p-region XPS spectrum corresponding to the MPC-Fe_3O_4 replica.

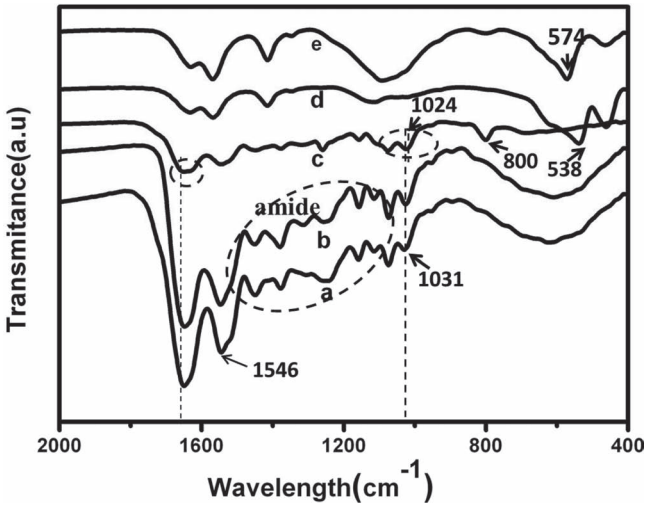

Figure 6. FTIR spectra of the original *Morpho* butterfly wing (a), the acid-treated butterfly wing (b), hybrid wings after dipping into the precursor (c), the PC-α-Fe_2O_3 replica (d) and the final product MPC-Fe_3O_4 replica (e).

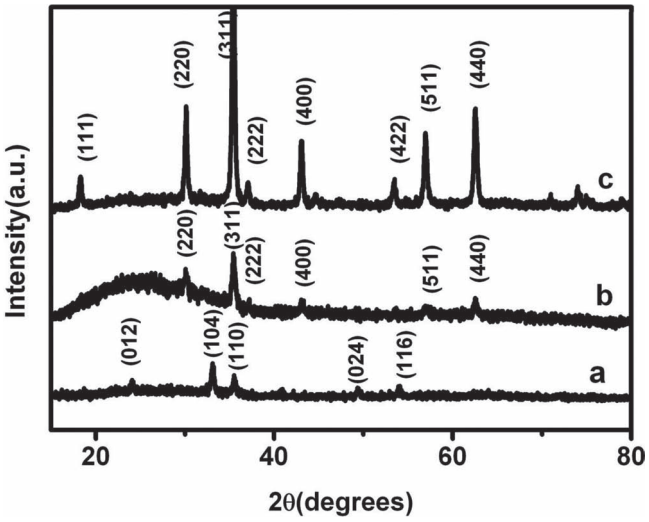

Figure 7. XRD patterns of the PC-α-Fe_2O_3 replica (a) and the MPC-Fe_3O_4 replica reduced at 400 °C (b) and 500 °C (c).

original butterfly wings. In addition, there was a new sharp band at 800 cm^{-1}, which indicates the binding of the Fe^{3+} with active groups on the chitin during the sol-gel and coating process. Thus, binding of the Fe^{3+} with the COOH/COO – groups of the chitin (COO…Fe^{3+})[30] and with the ring C–OH groups (C–O….Fe^{3+}) formed. The new band at 538 cm^{-1} was due to the vibrations of the Fe–O bonds in the crystalline lattice of the hematite (Fe_2O_3),[31] while the vibration of Fe–O bonds at 574 cm^{-1}[32] is characteristic of magnetite (Fe_3O_4). Therefore, the butterfly wing provided a reactive scaffold for the assembly of a precursor sol-gel solution from the micro- to the nanoscale, and thus the sol-gel could be coated homogeneously on the surface of the wing scales; this is supported by the SEM and TEM images and is consistent with the Raman spectra.

The reduction temperature also plays an important role in controlling the exact replication of the hierarchical structures in the MPC-Fe_3O_4. X-ray-diffraction (XRD) patterns of the obtained PC-α-Fe_2O_3 and the MPC-Fe_3O_4 reduced at 400 °C and 500 °C through the ferric chloride alcohol sol-gel route are compared in **Figure 7**. All of the recorded peaks in the PC-α-Fe_2O_3 can be assigned to hematite (JCPS no. 33-0664) without crystalline impurities. The diffraction peaks of the MPC-Fe_3O_4 reduced at 500 °C, at 30.01, 35.45, 37.08, 43.08, 53.45, 56.98, 62.57°, can be assigned to the (220), (311), (222), (400), (422), (511) and (440) planes of the Fe_3O_4, respectively (JCPS no. 65-3107). Unfortunately, the particles aggregated at this temperature, resulting in the collapse of the structures, as supported by SEM images (Figure S8, Supporting Information). When the reduction temperature was decreased to 400 °C, the diffraction peaks were identified to be Fe_3O_4. However, a broad peak from 20 to 30° was observed, attributed to the amorphous phase of the Fe_3O_4, because of the relatively low reduction temperature. Therefore, we chose 400 °C as the final reduction temperature to get the magnetite replica, because at this temperature the structural integrity of the replica could be maintained and most of the replica consisted of crystalline Fe_3O_4.

The successfully synthesized MPC and the corresponding intermediate products were also evidenced by optical images, as well as reflectance spectra, as shown in **Figure 8**. Reflection measurements were performed in the visible and near-IR regions to study the interaction of the synthesized replicas with light. The incident angle was vertical to the surface of the substrate. The reflectance spectrum of the original wing is also shown for comparison. The original butterfly wing exhibits its highest reflection at 400–460 nm (spectrum a in Figure 8A), which is in the violet-blue region of visible light. The relatively large reflectance in the short visible-wavelength region is consistent with its natural shining light-blue color, owing to its unique photonic-crystal structure.[33] The PC-α-Fe_2O_3 shows a distinct, red-shifted reflection peak at 650 nm (spectrum b in Figure 8A), which is consistent with the bright red color observed under optical microscopy (image b in Figure 8B). From the point of view that an obvious response to an imposed electromagnetic (EM) wave requires a large refractive-index (RI) difference between the two components of a PC, the appearance of this peak indicates that there must be a photonic band gap in the replicated structure, where the original, organic, lamellar lattice (chitin, RI = 1.56) was replaced with air and the Fe_2O_3 matrix, which has a higher RI (3.05). The final MPC-Fe_3O_4 replica displays reflection peaks at around 420, 525 and 645 nm (spectrum c in Figure 8A), although they have a somewhat-lower intensity than both the original butterfly wings and the PC-α-Fe_2O_3. The variations can be attributed to the different refractive indices of the replica constituents, and the magnetite particles, which have a refractive index of 2.4. The MPC-Fe_3O_4 gave blue, green or yellow colors under optical illumination (image c in Figure 8B). To the best of our knowledge, this is the first time that Fe_3O_4 with a hierarchical structure replicated from a butterfly wing has shown photonic properties. From the microstructures of the *Morpho* wing scales, we propose a model (inset in Figure 8C) to calculate the reflection spectra using a finite-difference time-domain (FDTD) model, and the calculated results are presented in Figure 8C. All of the parameters

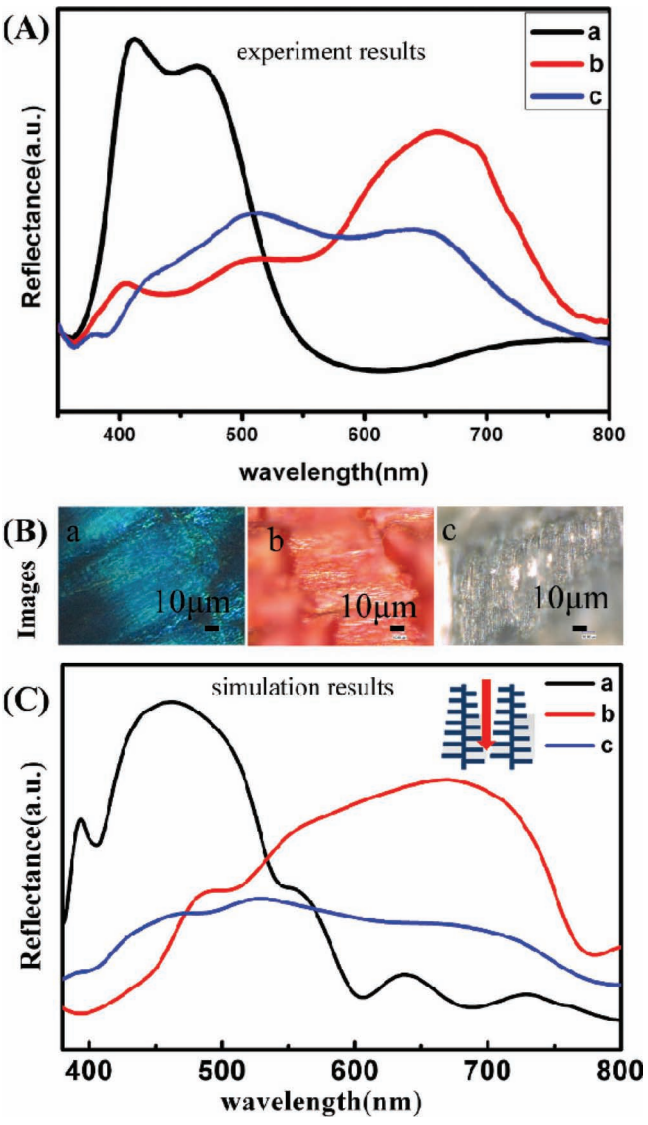

Figure 8. A) The reflection spectra of the original butterfly wing (a), the PC-α-Fe_2O_3 replica (b) and the final-product MPC-Fe_3O_4 replica (c) at normal incidence. B) The corresponding optical images. C) FDTD-simulation results of the original wing (a), the PC-α-Fe_2O_3 replica (b) and the final-product MPC-Fe_3O_4 replica (c). The inset shows the simulation model.

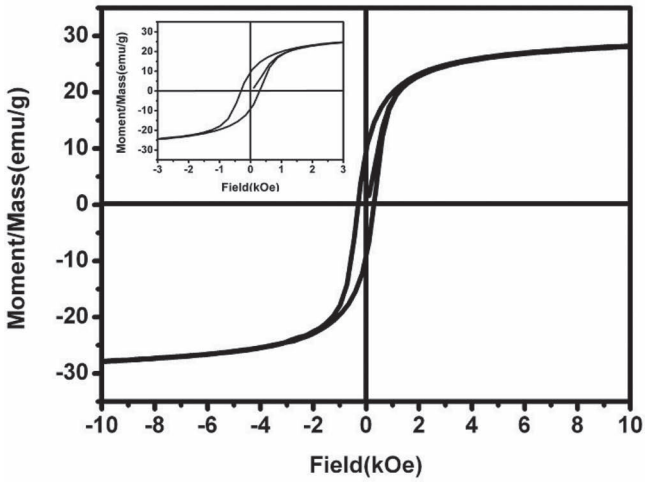

Figure 9. Magnetization loops of MPC-Fe_3O_4 obtained at a reduction temperature of 400 °C.

used in the calculation were obtained from the experiments. For the original *Morpho* butterfly wings, the calculated result is consistent with that of the measured spectrum (spectrum a in Figure 8A and 8C, black line), indicating the validity of our model. Furthermore, the experimental reflection data for both the PC-α-Fe_2O_3 (spectrum b in Figure 8A) and the MPC-Fe_3O_4 (spectrum c in Figure 8A) agree well with the calculated ones. It should be noted that the Fe_2O_3 and Fe_3O_4 particles in these replicas were of sub-micrometer dimensions: thus, additional diffuse reflection can be induced because of their granular surfaces. Moreover, the replica surface was not perfectly flat, which may also produce some deviations between the experimental and calculated results. According to these results, we found that a stronger modulation of the periodic sub-microstructure to visible EM waves was obtained with an increase in the RI. This modulation is a key characteristic of the structural colors, and thus is important to the application of PCs. Both the experimental and calculation results show that the reflection peak was red-shifted with the increase in the material RI, and the structure color was not sensitive to the layer thickness of the replica. Thus, different colors can be obtained simply by varying the RI, (i.e., using materials with different dielectric constants).

The magnetic properties of the MPC-Fe_3O_4 are shown in **Figure 9**. The magnetization curves were recorded using a vibrating-sample magnetometer (VSM) at room temperature. The VSM curve of the Fe_3O_4 replica prepared at 400 °C has a small coercive force of 299 Oe and a lower saturation magnetization of 29.2 emu g^{-1}; the MPC-Fe_3O_4 exhibits a nearly superparamagnetic behavior. We explored the optical and magnetic coupling effect between the inherited photonic crystal structure and the magnetite component further. The magnetic photonic functions could be observed clearly by studying the dependence of the diffraction wavelength on the strength of the external magnetic field (EMF). **Figure 10** shows typical reflection spectra of the MPC-Fe_3O_4 photonic crystals in response to a varying magnetic field, which was achieved by changing the distance between a NdFeB magnet and the sample from 4 to 6 cm. Two optical responses were explored: the main peak intensity at 525 nm decreased and the diffraction peak was slightly red-shifted from 645 to 673 nm as the strength of the magnetic field decreased (Figure 10B). At the same time, the color of the MPC-Fe_3O_4 changed from a mixture of blue and red to dark yellow (Figure 10A). Although the exact mechanism of the optical response is not clear, the external magnetic field affected the anisotropy of the Fe_3O_4. The color changes induced by the introduction of the EMF was due to the interaction between the magnetic Fe_3O_4 and the external field causing a distortion of the photonic crystal structure. The photonic crystal lattice distortion may be simulated using the FDTD model. It was found that, when the MPC-Fe_3O_4 photonic crystal shrank by 20% in the x-dimension and expanded 20% along the y-dimension

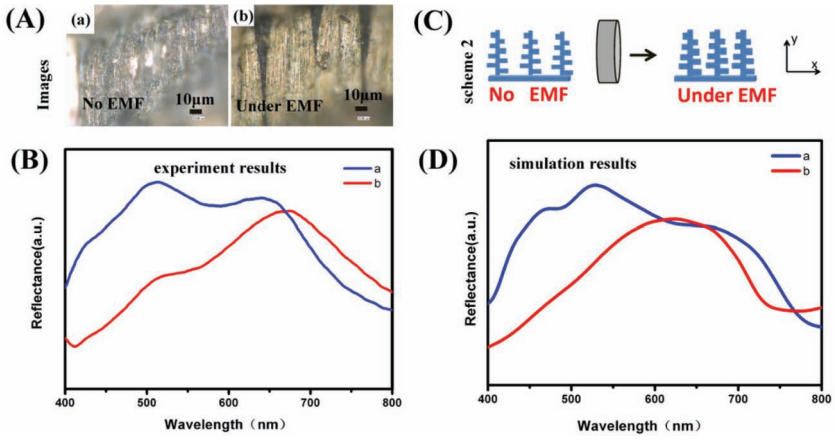

Figure 10. A) Optical images of the sample under no external magnetic field (EMF) (a) and under an EMF (b). B) The corresponding experimental reflection spectra at normal incidence. C) A schematic illustration of the changing process under an EMF. D) Optical simulation results.

(Figure 10C), the simulation reflection spectrum (Figure 10D) matched well with the experimental spectrum. The calculation clearly demonstrates that the MPC-Fe_3O_4 photonic crystal distorted under the stimulation of the EMF. We can conclude that the combined photonic crystal structure and the magnetite of MPC-Fe_3O_4 give rise to its magnetically tunable photonic properties.

3. Conclusions

In summary, a sol-gel then reduction process was successfully developed for the preparation of magnetophotonic crystal Fe_3O_4 from *Morpho* butterfly wings. The obtained MPC-Fe_3O_4 and the intermediate PC-α-Fe_2O_3 could reflect iridescent visible light, as evidenced from reflection spectroscopy and supported by theoretical calculations, suggesting that this process replicated not only the outer, but also the inner and more complex surfaces of the hierarchical structure of the butterfly wings. The sol-gel solution enhanced the structural integrity of the butterfly wing replicas through enhanced interactions between the active sites in chitin and the Fe^{3+} in the sol-gel solution. The resultant MPC-Fe_3O_4 demonstrated an optical and magnetic coupling effect and magnetically tunable photonic properties. The biologically derived magnetic photonic nanostructures open up an avenue for tunable magnetophotonic crystals, which may be useful for the creation of new magneto-optical devices and fundamental studies. Given the flexibility and the generality of the sol-gel templating and the wealth of known and as-yet-undiscovered complex biological photonic structures, their synergistic combination will offer unprecedented access to novel high-dielectric PCs with unique structures and superior optical properties.

4. Experimental Section

Preparation of the Iron Oxide Photonic Crystals: First, the ash content of the natural butterfly wings was removed by dipping them into a mixture of ethanol and acetic acid for 3 h in ambient conditions and then washing them thoroughly with deionized water and drying them in air for 12 h. After that, the pretreated wings were soaked in an iron chloride sol-gel solution for 24 h, which was prepared by dissolving $FeCl_3{\cdot}6H_2O$ in water-free ethanol, with a molar ratio of ethanol to $FeCl_3{\cdot}6H_2O$ of 1:0.3, at 60 °C for 15 min under magnetic stirring. Next, the soaked butterfly wings were taken out, washed with deionized water, and dried overnight at room temperature under vacuum. The chitin substrates were then removed by calcination at 500 °C for 3 h in air, leaving iron oxide in the form of ceramic butterfly wings. Samples thus prepared are denoted as photonic crystal Fe_2O_3 (PC-α-Fe_2O_3) replicas. Finally, magnetophotonic crystal Fe_3O_4 (MPC-Fe_3O_4) was obtained by the heat treatment of the PC-α-Fe_2O_3 under a H_2/Ar (1:4 volume ratio) flow at 400 or 500 °C for 3 h. As a comparison, Fe_3O_4 butterfly wings were also synthesized in the exactly same way as described above, except the $FeCl_3{\cdot}6H_2O$ precursor was replaced with aqueous Fe $(NO_3)_3{\cdot}9\ H_2O$.

Characterization: The XRD patterns of the samples were obtained using a Bruker-AXS X-ray diffractometer, using Cu K_α radiation. The Raman measurements were conducted using a Renishaw inVia Raman microscope, operated with an Ar-ion laser (514.5 nm). The XPS was carried out using a Physical Electronics PHI5400 instrument, using Mg K_α radiation as the X-ray source. The FTIR spectroscopy measurements were recorded using a Bruker EQUINOX 55 instrument. The FE-SEM images were obtained using an FEI Sirion 200 field-emission-gun scanning electron microscope, operated at an acceleration voltage of 5.0 kV. The TEM/HR-TEM measurements were made using a JEOL-2011F transmission electron microscope. Bright-field images, energy-dispersive X-ray (EDX) spectra and SAED patterns were obtained and examined. The magnetization measurements were performed using a vibrating sample magnetometer (VSM) (Lakeshore 7407) at room temperature. The optical micrographs of the samples were taken using a digital optical microscope (VHX-600, Keyence). The reflection measurements were made using a QDI 2010 UV–vis–near-IR micro-spectrophotometer.

Supporting Information

Supporting Information is available from the Wiley Online Library or from the author.

Acknowledgements

The authors gratefully acknowledge financial support for this research from the National Science Foundation of China (Nos. 51131004, 51171110, 51072117), the 973 national project (No. 2011CB922200), the Sino-French Project of the Ministry of Science and Technology (MOST) of China (No. 2009DFA52410), and the Shanghai Science and Technology Committee (No. 10JC1407600). The authors also thank the SJTU Instrument Analysis Center for the measurements.

Received: December 14, 2011
Published online: February 27, 2012

[1] S. John, *Phys. Rev. Lett.* **1987**, *58*, 2486.
[2] E. Yablonovitch, *Phys. Rev. Lett.* **1987**, *58*, 2059.
[3] E. Gavartin, R. Braive, I. Sagnes, O. Arcizet, A. Beveratos, T. J. Kippenberg, I. Robert-Philip, *Phys. Rev. Lett.* **2011**, *106*, 203902.
[4] S. W. Wang, W. Lu, X. S. Chen, Z. F. Li, X. C. Shen, W. J. Wen, *J. Appl. Phys.* **2003**, *93*, 9401.

[5] G. Wang, J. P. Huang, K. W. Yu, *Opt. Lett.* **2008**, *33*, 2200.
[6] C. Z. Fan, G. Wang, J. P. Huang, *J. Appl. Phys.* **2008**, *103*.
[7] J. D. Debord, L. A. Lyon, *J. Phys. Chem. B* **2000**, *104*, 6327.
[8] W. Park, J. B. Lee, *Appl. Phys. Lett.* **2004**, *85*, 4845.
[9] J. P. Ge, Y. X. Hu, Y. D. Yin, *Angew. Chem.* **2007**, *46*, 7428.
[10] M. J. Steel, M. Levy, R. M. Osgood, *J. Lightwave Technol.* **2000**, *18*, 1297.
[11] M. Inoue, R. Fujikawa, A. Baryshev, A. Khanikaev, P. B. Lim, H. Uchida, O. Aktsipetrov, A. Fedyanin, T. Murzina, A. Granovsky, *J. Phys. D: Appl. Phys.* **2006**, *39*, R151.
[12] T. Kodama, K. Nishimura, A. V. Baryshev, H. Uchida, M. Inoue, *Phys. Status Solidi B* **2004**, *241*, 1597.
[13] M. Inoue, H. Uchida, K. Nishimura, P. B. Lim, *J. Mater. Chem.* **2006**, *16*, 678.
[14] P. N. Bartlett, M. A. Ghanem, I. S. El Hallag, P. de Groot, A. Zhukov, *J. Mater. Chem.* **2003**, *13*, 2596.
[15] J. P. Ge, Y. P. Hu, T. R. Zhang, T. Huynh, Y. D. Yin, *Langmuir* **2008**, *24*, 3671.
[16] J. P. Ge, L. He, J. Goebl, Y. D. Yin, *J. Am. Chem. Soc.* **2009**, *131*, 3484.
[17] P. Vukusic, J. R. Sambles, *Nature* **2004**, *429*, 680.
[18] S. Lei, H. W. Yin, R. Y. Zhang, X. H. Liu, J. Zi, D. Y. Zhao, *J. Mater. Chem.* **2010**, *20*, 90.
[19] J. W. Galusha, M. R. Jorgensen, M. H. Bartl, *Adv. Mater.* **2010**, *22*, 107.
[20] R. C. McPhedran, N. A. Nicorovici, D. R. McKenzie, L. C. Botten, A. R. Parker, G. W. Rouse, *Aust. J. Chem.* **2001**, *54*, 241.
[21] J. Nozawa, K. Tsukamoto, W. V. Enckevort, T. Nakamura, Y. Kimura, H. Miura, H. Satoh, K. Nagashima, M. Konoto, *J. Am. Chem. Soc.* **2011**, *133*, 8782.
[22] W. Zhang, D. Zhang, X. T. Fang, J. J. Gu, J. Ding, H. Wang, Q. X. Guo, H. Ogawa, *Chem. Mater.* **2009**, *21*, 33.
[23] Y. Chen, X. N. Zang, J. J. Gu, S. M. Zhu, H. L. Su, D. Zhang, X. B. Hu, Q. Liu, W. Zhang, D. X. Liu, *J. Mater. Chem.* **2011**, *21*, 6140.
[24] Y. Chen, J. J. Gu, S. M. Zhu, T. X. Fan, D. Zhang, Q. X. Guo, *Appl. Phys. Lett.* **2009**, *94*, 053901.
[25] S. Yoshioka, S. Kinoshita, *Proc. R. Soc. London B: Biol. Sci.* **2004**, *271*, 581.
[26] J. Y. Huang, X. D. Wang, Z. L. Wang, *Nano Lett.* **2006**, *6*, 2325.
[27] R. M. Cornell, U. Schwertmann,*The Iron Oxides: Structure, Properties, Reactions, Occurences and Uses*, 2nd ed., Wiley-VCH, Weinheim, Germany **2003**, Ch. 7.
[28] A. P. Grosvenor, B. A. Kobe, M. C. Biesinger, N. S. McIntyre, *Surf. Interface Anal.* **2004**, *36*, 1564.
[29] J. S. Church, G. L. Corino, A. L. Woodhead, *Biopolymers* **1997**, *42*, 7.
[30] J. Araña, O. González Dıíaz, J. M. Doña Rodrıíguez, J. A. Herrera Melián, C. Garriga i Cabo, J. Pérez Peña, M. Carmen Hidalgo, J. A. Navıío-Santos, *J. Mol. Catal. A: Chem.* **2003**, *197*, 157.
[31] B. Pal, M. Sharon, G. Nogami, *Mater. Chem. Phys.* **1999**, *59*, 254.
[32] M. Ma, Y. Zhang, X. B. Li, D. G. Fu, H. Q. Zhang, N. Gu, *Colloids Surf. A: Physicochem. Eng. Aspects* **2003**, *212*, 219.
[33] L. P. Biró, K. Kertész, Z. Vértesy, G. I. Márk, Z. Bálint, V. Lousse, J. P. Vigneron, *Mater. Sci. Eng. C* **2007**, *27*, 941.